Aberystwyth University

Direct and Accurate Feature Extraction from 3D Point Clouds of Plants Using RANSAC

Morteza Ghahremani*,† Kevin Williams‡ Fiona Corke‡ Bernard Tiddeman*,
Yonghuai Liu§ Xiaofeng Wang¶

Abstract

While point clouds hold promise for measuring the geometrical features of 3D objects, their application to plants remains problematic. Plants are three dimensional (3D) organisms whose morphology is complex, varies from one individual to another and changes over time. Objective measurement of attributes in 3D point cloud domain is increasingly attractive as techniques improve the accuracy and reduce computational time. Analysis of point cloud data, however, is not straightforward, due to its discrete nature, imaging noise and cluttered background. In this paper, we introduce a robust method for the direct analysis of plants of point cloud data. To this end, we generalise the random sample consensus (RANSAC) algorithm for the analysis of 3D point cloud data and then use it to model different plant organs. Since 3D point clouds are obtained from multi-view stereo images, they are often contaminated with a considerable level of noise, distortions and out-of-distribution points. Key to our approach is the use of the RANSAC algorithm on 3D point cloud, making our technique more robust to undesirable outliers. We tested our proposed method on Brassica and grapevine by comparing the estimated measurements extracted from the models with manual ones taken from the actual plants. Our proposed method achieved $R^2 > 0.90$ for measured diameters of branches and stems in Brassica while it yielded $R^2 > 0.91$ for the measured leaf angles of grapevine and branch angles of Brassica. In all cases, the approach produced stable performance under imaging noise and cluttered background while the conventional methods often failed to work.

Keywords: Point cloud; 3D analysis; Random sample consensus (RANSAC); Brassica; Grapevine

1 Introduction

Measuring attributes of biological organisms in three dimensional (3D) space is a challenging topic that has attracted much attention in recent years. Such measurements have the potential to reveal more reliable information about the organism, including its behaviour across time. Although measurements taken from 2D images are still useful for many purposes [1; 2], the lack of depth information can lead to challenges/ambiguity in interpretation. Recent technical advances in 3D imaging enable more cost-effective data acquisition and accurate rapid modelling [3; 4; 5]. However, 3D analysis and modelling remain a relatively complex process, and despite the potential importance to plant science, only a few methods have been developed for 3D point clouds, most of which require very specific conditions and cannot be extended to the large datasets required for agronomy and genetics.

Previous 3D studies tend to have used derived volumetric grids rather than the point cloud produced directly from many acquisition methods. Volumetric grids represent digitized 3D data as voxels, whereas point clouds are composed of unordered points. Many modelling methods produce point clouds as their primary output, but these can be challenging to manipulate computationally and tend to be transformed firstly into mesh, regular voxels or 2D grids [6; 7; 8; 9]. However, data transformations are often accompanied with quantization artefacts and lead to loss of inherent geometric information contained in the original 3D point cloud data. High complexity is another drawback of the data representation transformations. That said, point clouds are relatively primitive in representation and their unified structures do not need the combinatorial irregularities and complexities of meshes or volumetric voxels, making subsequent analysis and

---

*Department of Computer Science, Aberystwyth University, United Kingdom

†mog9@aber.ac.uk

‡National Plant Phenomics Centre, Institute of Biological, Environmental and Rural Sciences, Aberystwyth University, Aberystwyth, United Kingdom

§Department of Computer Science, Edge Hill University, United Kingdom

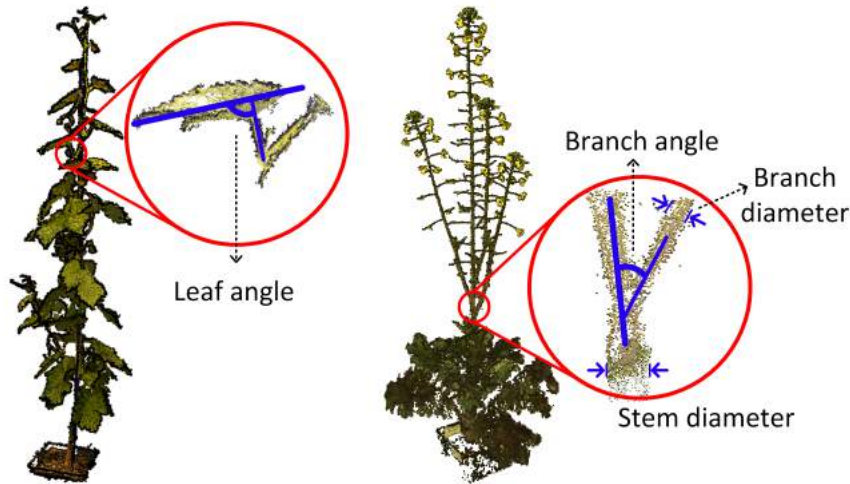¶School of Information Science & Technology, Northwest University, China

Figure 1: 3D phenotyping of grapevine (left) and Brassica (right) in the 3D point cloud.

feature extraction potentially faster. Several studies [10; 11; 12; 13; 14; 15; 16] demonstrate segmentation and skeletonization directly from point clouds. The processed data is then used for measuring parameters of interest, including diameters of different organs, branching angles and leaf angles as shown in Fig. 1. Such parameters are still measured manually or semi-automatically [17; 18; 19], require specific conditions and are often contaminated by imaging noise, distortion and out-of-distribution points in the data acquisition process.

The goal of this study is to propose an improved method for processing such data generated using representative structure from motion techniques [20; 21; 22], 3D laser scanners [23], LiDAR [24], etc.

In this paper, we propose a novel method for accurately analysing point cloud data using random sample consensus (RANSAC). We provide both a theoretical and experimental evaluation of our approach. We show that our method can approximate diameters and angles of point clouds of plants accurately even in the presence of noise and irrelevant data. The theoretical analysis illustrates how our method is highly robust to perturbation of the input points as well as to corruption from outliers or imaging noise. The rest of this paper is organized as follows. Section 2 reviews existing 3D phenotyping methods. The proposed RANSAC-based method is detailed in Section 3, and Section 4 reports and discusses the experimental results of our method on Brassica and grapevine datasets. Finally, conclusions and future work are provided in Section 5.

2   Background

Angle and thickness of organs are important traits that determine important aspects of plant architecture, growth, and yield. Leaf angle influences light interception and water relations. Variation of leaf angle can contribute to water stress tolerance [17] while leaf erectness can increase light absorption, improve photosynthetic assimilation, and allow high density planting in crops such as rice [25]. The thickness of organs can contribute to mechanical strength, notably in cereals where stem diameter may be important in lodging [26]. Xu *et al.* [27] showed that the ratio of stem diameter to plant height in soybeans is a useful indicator for analyzing their lodging resistance. A similar metric was reported in [28] that estimates the amount of mass produced of sorghum. Melese *et al.* [29] showed a linear relationship between root tensile strength and its diameter. In many plant species, measuring branch angles is an important trait in crop breeding [30]. Li *et al.* [31] investigated the relationship between branch angle and the elevation of branch position in Brassica. Bemer *et al.* [32] discovered that branch angles in Arabidopsis are affected by light conditions. Branch and leaf behaviour have been considered as effective parameters in phenotyping and trait analysis of various plant species [33; 34; 35; 36]. Thus, the accurate rapid measurement of parameters such as diameters and branch angles is desirable both for agronomic management of crops as well as for breeding superior varieties. This study focuses on accurate estimation of angle and diameter parameters of plants from their point clouds built using typical structure from motion techniques [20; 21; 22], 3D laser scanners [23], or LiDAR [24].

Angle measurement in plant science is a challenging task due to the high complexity of organs and their variability. Angles may be measured manually using instruments such as inclinometers or goniometers but that is labour intensive. Non-contact measurements facilitate scale up for research, potentially allowing many

individuals to be followed across their life cycle, providing information on how their attributes change over time and in response to their environment. Non-contact measurement using non-destructive sensors could also improve crop management strategies by providing near real-time assessment of plant health. Pisek *et al.* [37] measured the leaf angles from 2D images using the ImageJ* software, assuming that leaf azimuth orientation has a uniform distribution. 3D data could provide improved accuracy due to inherent depth information that is missing from 2D images. In the following, we review the techniques developed for 3D data.

Let $\mathbf{P}$ denote the point cloud of a plant's organ. It includes such organs as stem, leaf, petiole, etc, centred at the origin of the 3D Cartesian coordinate. The goal is to model the given point cloud $\mathbf{P}$ by fitting an appropriate geometrical shape $\mathbf{C}$ that satisfies

$$\arg \min_{\mathbf{C}} \sum_{i=1}^{N} ||\mathbf{P}_i - \mathbf{C}||_2^2, \tag{1}$$

where N is the number of points and '$||.||_2$' denotes the L_2-norm. If $\mathbf{C}$ is assumed as a plane, solving this equation yields $\hat{\mathbf{C}} = \frac{1}{N} \sum_{i=1}^{N} \mathbf{P}_i$, which is an average of points, and its corresponding normal vector is obtained as $\overrightarrow{n}_{\mathbf{C}} = \hat{\mathbf{C}}/||\hat{\mathbf{C}}||_2$. This solution, however, fails to estimate a valid orientation vector and is not applicable to point clouds in practice.

Briglia *et al.* [17] approximated the leaf blade regression plane and petiole regression line of point cloud data using CloudCompare† and point cloud library (PCL)‡. Lou *et al.* [38] used a 3D bounding-box approach for estimating branching angles in Arabidopsis point clouds. A 3D bounding-box consists of eight corners that surround the points within a small neighbourhood of the point of interest. Several studies [18; 39; 40; 13; 41] consider the following minimization problem:

$$\arg \min_{\mathbf{C}} ||\mathbf{\Phi}^T \mathbf{C}||_2^2. \tag{2}$$

In this equation, matrix $\mathbf{\Phi}$ is the singular value decomposition (SVD) of the zero-mean point set $\mathbf{P}$ and it is represented as $\mathbf{U}_{3\times3}\mathbf{S}_{3\times N}\mathbf{V}_{N\times N}^T$, where $\mathbf{U}$ and $\mathbf{V}$ are eigenvector matrices and $\mathbf{S}$ is the eigenvalue matrix. The normal vector of the above optimization is obtained via $\overrightarrow{n}_{\mathbf{C}} = \mathbf{U}(...,3)$. Though the SVD-based results are more reliable than the averaging ones, it is not applicable to organs with a highly complex structure.

The main drawback of all the above-mentioned techniques is a failure to appropriately model the structural information of organs, especially those with high complexity. During fitting a model to an organ, outliers influence the estimated parameters and removing them from the computation can result in a better fit of the model. In this work, we model plant organs as cuboids and cylinders, and remove the effects of outliers by a point cloud RANSAC. RANSAC can tolerate up to 50% outliers [42; 43], resulting in robust model estimation against undesirable outliers.

3   Proposed Point Cloud RANSAC Algorithm for 3D Phenotyping

RANSAC [43] is an iterative method to estimate the mathematical model parameters of a set of observed data. The underlying concept of RANSAC is to exclude outliers from a given set and then fit the model to the remaining data (called inliers). Here, we introduce 3D RANSAC, suitable for analysis of point cloud data. The main properties of the proposed point cloud RANSAC (PC-RANSAC) are

- It has a conceptually simple structure, making it feasible for dealing with large, complex and variable point cloud datasets.

- It is easy to model any desired plant organ and is easily extensible to a wide range of plants.

- It can deal with distorted point clouds containing even more than 50% outliers.

We tested the approach by measuring the diameters and angles of architecturally distinct plants. Examples are shown in Figs. 2(a) and 2(b). Our approach starts by modelling appropriate geometrical shapes, cuboids and cylinders, for different plant parts (Section 3.1). The next stage is to fit the model onto an organ (the stem and the branch in Fig. 2(a) or the leaf and the petiole in Fig. 2(b)) using PC-RANSAC. As will be discussed in Section 3.2, PC-RANSAC decomposes the point clouds into inlier and outlier points,

---

*https://imagej.nih.gov/ij/
†https://www.danielgm.net/cc/
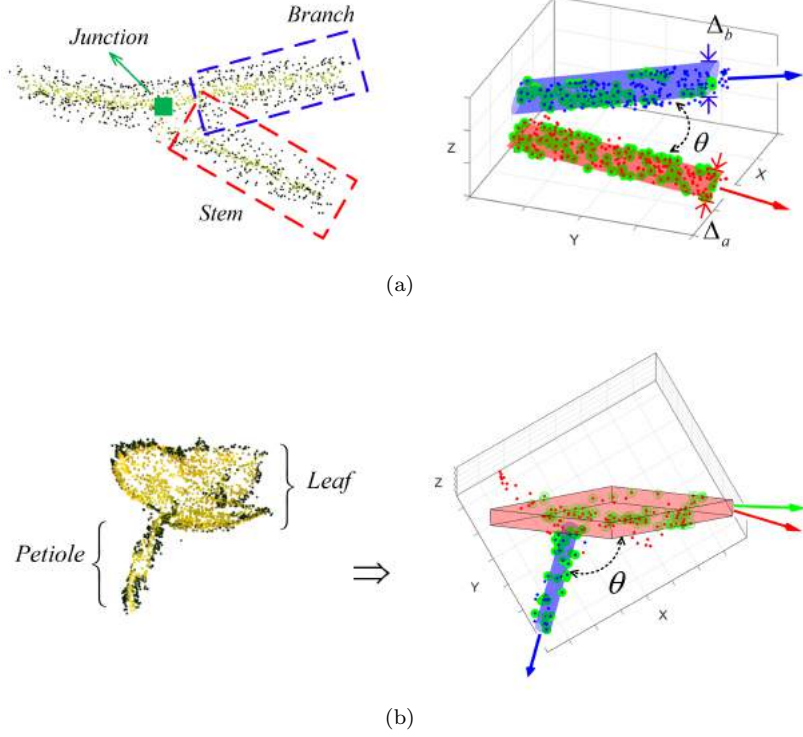‡https://pointclouds.org/

Figure 2: 3D phenotyping of Brassica (a) and grapevine (b) in the 3D point cloud. The outliers of PC-RANSAC are shown by the red and the blue dot points, and the ones encircled by green circles are inliers. Only inlier points are used in the estimation of the model parameters.

and the favourable inliers, shown in green in Fig. 2, are then employed for the estimation of an underlying model's parameters. Outlier points are discarded as they are less relevant for representing and estimating the parameters of an underlying organ. This strategy makes the proposed technique robust against point perturbation, out-of-shape distributed points and imaging noise introduced in the process of point cloud reconstruction. Finally, the estimated models are used for extracting parameters of interest including angles (Section 3.3) and diameters (Section 3.4) of Brassica and grapevine respectively.

Notation: A branching area in Brassica can be classified into a junction, a stem and a branch, as shown in Fig. 2(a). The stem is denoted by point cloud $\mathbf{P}_a = \{\mathbf{p}_{a,1}, ..., \mathbf{p}_{a,n}\}$, where '$n$' is the number of 3D points which are each defined as a 3×1 vector $\mathbf{p} = [p_x, p_y, p_z]^T$ ('T' is transpose). Likewise, a branch point set with m points is denoted by $\mathbf{P}_b = \{\mathbf{p}_{b,1}, ..., \mathbf{p}_{b,m}\}$. The parameters of interest are an angle θ between the stem and the branch and their diameters Δ. A petiole and a leaf in grapevine [Fig. 2(b)] are denoted as $\mathbf{P}_a = \{\mathbf{p}_{a,1}, ..., \mathbf{p}_{a,n}\}$ and $\mathbf{P}_b = \{\mathbf{p}_{b,1}, ..., \mathbf{p}_{b,m}\}$ respectively, and the angle (θ) restricted by these organs is unknown and must be estimated.

3.1 Shape representation

We focus on cuboid and cylinder shapes in this study [Fig. 3(a)] but the extension to other shapes is straightforward and can be found in [44; 45; 46; 47].

Cylinder shape: A cylinder is described by 3 parameters: orientation axis $\overrightarrow{n}$, the point on the axis $\mathbf{p}_{\overrightarrow{n}}$ and radius r. A point set $\{\mathbf{p}_1, \mathbf{p}_2, \mathbf{p}_3\}$, where the points are not colinear, will lie in a plane. Two normalised difference vectors $\overrightarrow{n}_1$ and $\overrightarrow{n}_2$ within the plane are given by

$$\overrightarrow{n}_1 = \frac{\mathbf{p}_2 - \mathbf{p}_1}{||\mathbf{p}_2 - \mathbf{p}_1||_2}, \overrightarrow{n}_2 = \frac{\mathbf{p}_3 - \mathbf{p}_1}{||\mathbf{p}_3 - \mathbf{p}_1||_2}. \tag{3}$$

They are of size 3×1. To generate a cylinder from two points with their corresponding normalised difference vectors, i.e. $\{(\mathbf{p}_{\overrightarrow{n}_1}, \overrightarrow{n}_1), (\mathbf{p}_{\overrightarrow{n}_2}, \overrightarrow{n}_2)\}$, the orientation axis $\overrightarrow{n}_z$ is first computed via

$$\overrightarrow{n}_z = \overrightarrow{n}_1 \times \overrightarrow{n}_2. \tag{4}$$
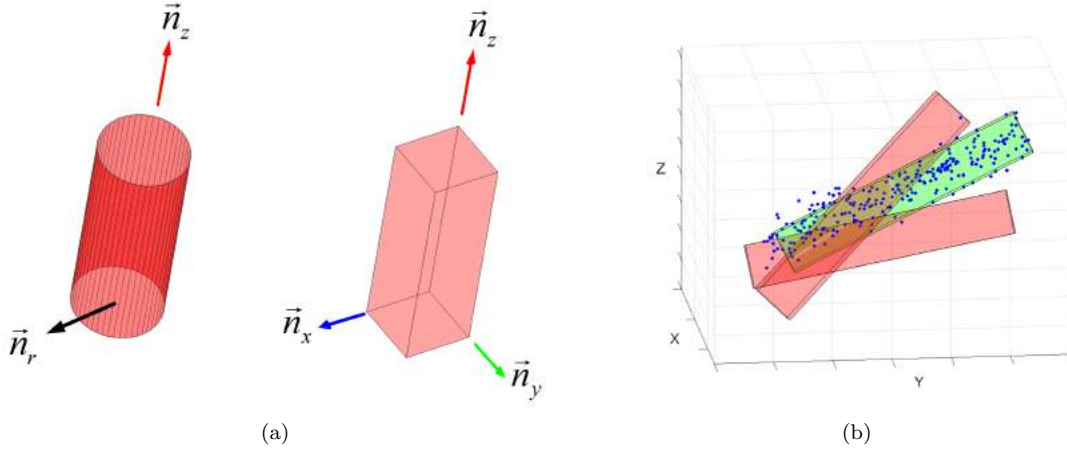
4

Figure 3: Applied models in PC-RANSAC; left: cylinder, right: cuboid. (b) PC-RANSAC fits the given models in Fig. 3(a) into a point cloud randomly and then selects the optimal solution (shown as a green cuboid) that includes the highest number of points and discards sub-optimal solutions, illustrated in red. Model parameters are finally estimated using the points approximated by the optimal solution.

Then the two parametric lines $\mathbf{p}_{\overrightarrow{n}_1}+t\overrightarrow{n}_1$ and $\mathbf{p}_{\overrightarrow{n}_2}+t\overrightarrow{n}_2$ along the axis are projected onto the plane $\overrightarrow{n}_z \cdot x = 0$ and their intersection is centred at $\mathbf{p}_c$. The radius of the cylinder r is equal to the distance between $\mathbf{p}_c$ and $\mathbf{p}_{\overrightarrow{n}_1}$ in that plane.

Cuboid shape: As shown in Fig. 3(a), a rectangular cuboid is represented by eight corner points $\mathbf{C} = \{C_1, ..., C_8\}$ [48]. To generate these parameters, we need three perpendicular planes. We derive our cuboid from a point set that includes three points with their corresponding normalised difference vectors $\{(\mathbf{p}_{\overrightarrow{n}_1}, \overrightarrow{n}_1), (\mathbf{p}_{\overrightarrow{n}_2}, \overrightarrow{n}_2), (\mathbf{p}_{\overrightarrow{n}_3}, \overrightarrow{n}_3)\}$, where any two arbitrary points are not laid in the same plane. The intersection of all the planes is centred at $\mathbf{p}_c$ and computed as follows:

$$\mathbf{p}_c = \frac{(\mathbf{p}_{\overrightarrow{n}_1} \cdot \overrightarrow{n}_1)(\overrightarrow{n}_2 \times \overrightarrow{n}_3)}{(\overrightarrow{n}_1 \times \overrightarrow{n}_2) \cdot \overrightarrow{n}_3} + \frac{(\mathbf{p}_{\overrightarrow{n}_2} \cdot \overrightarrow{n}_2)(\overrightarrow{n}_3 \times \overrightarrow{n}_1)}{(\overrightarrow{n}_1 \times \overrightarrow{n}_2) \cdot \overrightarrow{n}_3} + \frac{(\mathbf{p}_{\overrightarrow{n}_3} \cdot \overrightarrow{n}_3)(\overrightarrow{n}_1 \times \overrightarrow{n}_2)}{(\overrightarrow{n}_1 \times \overrightarrow{n}_2) \cdot \overrightarrow{n}_3}. \tag{5}$$

Since the normal vectors of the planes are perpendicular, the orientation axes correspond to the planes' normal vectors.

3.2 Estimation of shape parameters by point cloud RANSAC (PC-RANSAC)

We define γ as the minimum number of points required for the estimation of a model. Parameter γ depends on the type of the applied shapes discussed in the preceding section. Each normal vector needs three points that are not colinear so, it is 6 for a cylinder and 9 for a cuboid. Since the points may lie in the same line, two or three additional points are typically considered during computation. The concept of PC-RANSAC is to search and select γ points from a point cloud that fit well into a given model. It selects points randomly and then computes the parameters of the corresponding model. The next step is to detect all the points that are approximated by the computed model and label these as inliers. The process of point selection, model computation and inliers counting are repeated k times. In each iteration, the number of detected inliers is compared to that in the previous one and if the new result is better, it will be stored as the best answer. The inliers are selected by their distance and normal vectors, and since this process is recursively updated it removes outliers and noisy points, yielding an accurate estimation of model parameters. Fig. 3(b) exemplifies these steps, where PC-RANSAC seeks model parameters that maximize the number of inliers.

The number k of iterations is often determined by the a priori probability of inliers over the whole points. If the number of inliers and input points are denoted by n_i and n_s respectively, then the probability of randomly selecting a point as an inlier is equal to $P(n_i) = n_i/n_s$. The maximum number k of iterations must be large enough that satisfies $P(n_i, k) \geq 0.99$ [49]. The objective probability to find a subset that does not include any inliers $\left(1 - P^\gamma(n_i)\right)$ after k iterations is thus:

$$P(n_i, k) = 1 - \left(1 - P^\gamma(n_i)\right)^k. \tag{6}$$

5

The maximum number k of iterations that can be derived from the above equation is then:

$$k \geq \frac{\log\left(1 - P(n_i, k)\right)}{\log\left(1 - P^\gamma(n_i)\right)}, \tag{7}$$

where $P(n_i, k)$ is greater than a predetermined threshold P_t. P_t usually takes a value between 0.9 and 0.99 [49] and is set to 0.99 in this study. For cuboid shapes with γ equal to 9, it yields $k_{min} = 2355$ according to Eq. 7. More precisely, a cuboid model needs to be applied at least 2355 times recursively to the given point clouds and the one with the most inliers is selected as the resultant optimal one. We summarize the PC-RANSAC as follows:

1. Randomly select the minimum number γ of points required for estimation of the model. Parameter γ depends on the type of the applied model described in the preceding section.

2. Compute the shape parameters.

3. Determine how many points from the point cloud are approximated by the computed shape in Step 2.

4. Label the points inside the shape as inliers and the rest as outliers.

5. Repeat Steps 1 through 4 until the number of iterations is greater than the predetermined value.

6. Select the subset with the largest number of inliers.

7. Compute the model parameters from the given largest subset.

3.3 Angle measurement

Each predicted shape model in the 3D domain contains three orientation values, known as yaw, pitch and roll, represented as $\Theta = [\theta_{yaw}, \theta_{pitch}, \theta_{roll}]^T$. We are given two orientation vectors $\{\Theta_a, \Theta_b\}$ obtained by PC-RANSAC described in the preceding section as input and the goal is to compute the angle between these two vectors. To this end, we first convert each orientation vector into a 3×3 rotation matrix, $\mathbf{R}^{3\times3}$, using the Rodrigues formula [50] and then flatten§ them to compute their angle via

$$\theta = cos^{-1}\left(\frac{<\mathbf{R}_a^F, \mathbf{R}_b^F>}{||\mathbf{R}_a^F||_2 \, ||\mathbf{R}_b^F||_2}\right), \tag{8}$$

where superscript F denotes the flatten operator.

3.4 Diameter measurement

For the cuboid model, the diameter Δ of different parts of a plant could be computed by the shape normal vectors $\overrightarrow{n} = [\overrightarrow{n}_x, \overrightarrow{n}_y, \overrightarrow{n}_z]^T$, the intersection point $\mathbf{p}_c$ and the inlier set $\mathbf{P}_i$ with n_i points. We project each inlier point onto the shape normal vector and then extract the diameter via

$$\Delta_a = \max_i\{(\mathbf{P}_{a,i} - \mathbf{p}_c) \cdot [\overrightarrow{n}_x, \overrightarrow{n}_y, 0]^T\}, \quad i = 1, ..., n_i \tag{9}$$

$$\Delta_b = \max_i\{(\mathbf{P}_{b,i} - \mathbf{p}_c) \cdot [\overrightarrow{n}_x, \overrightarrow{n}_y, 0]^T\}, \quad i = 1, ..., m_i, \tag{10}$$

where Δ_a and Δ_b are the diameters of a stem and a branch, respectively. In the cylinder model, we first determine the lines crossing the centres of its two bases (represented as L) and then compute the diameter

$$\Delta_a = \max_i\{(\mathbf{P}_{a,i} - \mathbf{L}) \cdot [\overrightarrow{n}_x, \overrightarrow{n}_y, 0]^T\} - \min_i\{(\mathbf{P}_{a,i} - \mathbf{L}) \cdot [\overrightarrow{n}_x, \overrightarrow{n}_y, 0]^T\}, \quad i = 1, ..., n_i, \tag{11}$$

$$\Delta_b = \max_i\{(\mathbf{P}_{b,i} - \mathbf{L}) \cdot [\overrightarrow{n}_x, \overrightarrow{n}_y, 0]^T\} - \min_i\{(\mathbf{P}_{b,i} - \mathbf{L}) \cdot [\overrightarrow{n}_x, \overrightarrow{n}_y, 0]^T\}, \quad i = 1, ..., m_i. \tag{12}$$

---

§The flatten operator converts any 2D matrix to a 1D vector with values taken row-wise.

In order to increase the reliability of the measurements, we repeat all the above steps $20 < R < 50$ times and the median of the results is selected as the final estimate. The number R of repetition depends on the complexity of plants and their point clouds. The pseudocode of the proposed point cloud phenotyping technique is summarised as Algorithm 1.

Algorithm 1: The proposed method for phenotyping plants in point cloud

---

• Partition the given point cloud around a junction/node into two clusters $\{\mathbf{P}_a, \mathbf{P}_b\}$ containing a stem and a branch or a petiole and a leaf;
• Select the model discussed in Section 3.1 and set thresholds and recursion parameters including γ, P_t, k_{min} and R;
• Initialize: $counter=1$, $\Theta \leftarrow \emptyset$ {computed angles} and $\Delta \leftarrow \emptyset$ {computed diameters};
• **while** $counter \leq R$:
    1- **for** each cluster **do**:
        Apply PC-RANSAC (Section 3.2) to extract the given model parameters;
     end for
    2- Compute the angle θ of the given junction/node through Eq. 8;
    3- Compute the diameters $\{\Delta_a, \Delta_b\}$ of the given organs through Eqs. 9 and 10;
    4- $\Theta \leftarrow \theta$, $\Delta \leftarrow \{\Delta_a, \Delta_b\}$;
    5- Increase $counter$ by 1;
end while
• Return the medians of the measurement sets $\{\theta, \Delta_a, \Delta_b\}$.

---

4 Experimental Results

We validate our method over a Brassica and a grapevine dataset as detailed in Section 4.1. In short, each dataset was split into three *easy*, *moderate* and *difficult* tasks to verify the performance and robustness of the proposed technique under different conditions. The accuracy of the results was computed by the Pearson correlation coefficient (CC) and relative root mean square error (RRMSE). Section 4.2 evaluates our technique against averaging as a baseline and the existing methods including SVD and bounding-box over both noisy and noise-free data. Finally, an ablation study for the parameters of PC-RANSAC and the time cost are provided in Section 4.3.

4.1 Data acquisition

37 diverse genotypes of Brassica, comprising part of Experiment BR017, were used to acquire the images for modeling. The plants were grown and imaged in the 2 conveyor compartments on the Lemnatec system in National Plant Phenomics Centre [¶]. Seeds were sown in 400ml pots of Levington F2 peat-based compost and grown for 3 weeks before being exposed to cold (either 5^oC or 10^oC with daylength of 10 hours for 6 weeks). After the cold treatment plants were transferred to 3.5L capacity pots of Levington M3 peat-based compost. Once the plants were settled in the larger pots they were transferred to a conveyor based automated watering and imaging system (Lemnatec, Germany) at NPPC and grown under 600W HPS luminaries at a light level of 300 μM m^{-2} s^{-1}. Pots were watered daily to a target weight equivalent 75% soil water content. Plants were grown on the conveyor system until maturity. Grafted grapevines (variety Aleatico) were obtained from Italy and grown as previously described in [17]. Plants were potted in 3.5L pots of a 50/50 mixture of soil based compost and grit sand with added lime. Plants were grown on a bespoke gravimetric system that ensures consistent water availability to the plants. Plants had been pruned to remove excessive young growth and grown for 2 years prior to the measurements.

In this study, we used 178 Brassica and 21 grapevine image sets collected at NPPC using a PhenoGreen rotary table for capturing 60 high-resolution multi-view images (6000×4000 px.) per plant. The images were then fed into COLMAP[‖] for reconstructing their 3D models. In short, the structure-from-motion (SfM) algorithm [51] extracts the calibration parameters (intrinsic and extrinsic matrices) from the images, and the images are then projected into the 3D domain by the multi-view stereo (PMVS) algorithm [51]. The number of points in the reconstructed point cloud data varies from $500K$ to $2,500K$ points, depending on the plants' dimensions. We manually annotated the point clouds using the MeshLab[**] software, where the

---

Table 1: Details of the number of samples per dataset used in this study

Dataset	#Easy	#Moderate	#Difficult
Brassica	235	158	107
Grapevine	87	46	38

junction regions were split into a stem and a branch in Brassica and a petiole and a leaf in grapevine. Regions of interest were extracted and categorized into one of three categories - *easy*, *moderate* and *difficult*. The details of the manually annotated point clouds are tabulated in Table 1 and examples are shown in Figs. 4(a) and 4(b). Easy samples contain few or no outliers while difficult samples contain a large number of outliers (maximally 10%) that arise during the 3D reconstruction. Difficult samples may also present some irregularities in appearance, making the estimation process more challenging. The amount of outliers in 3D models may exceed 10% due to low-resolution sensors, highly occluded samples, imaging conditions etc but this amount of outliers is usually an upper bound of outliers in our reconstructed point clouds.
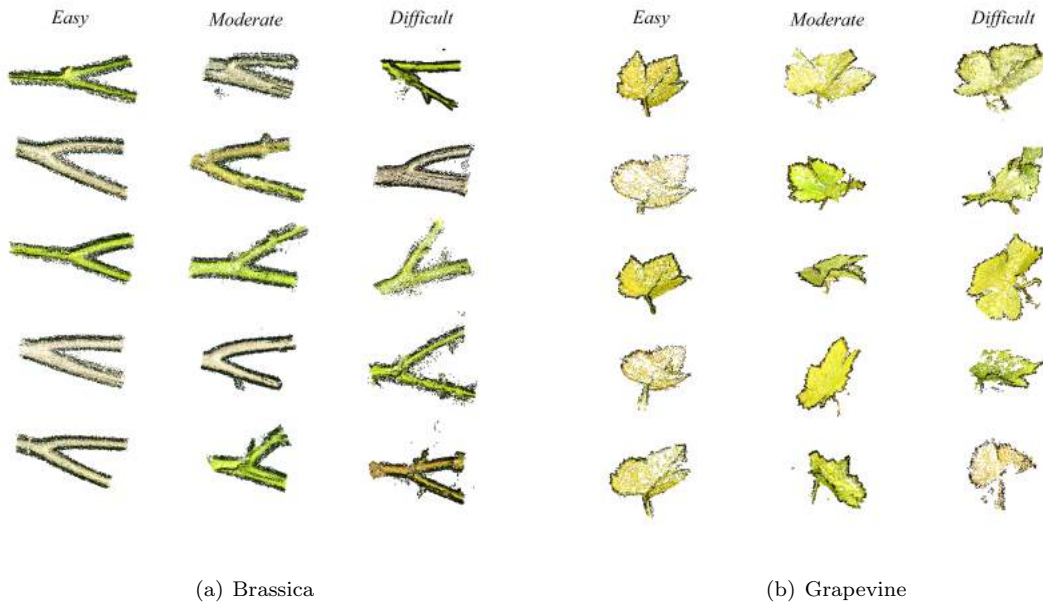

(a) Brassica
(b) Grapevine

Figure 4: Examples of extracted junction regions from the Brassica and grapevine datasets, categorized into easy, moderate and difficult samples.

4.2 Results and discussion

In our method, the branches and stems of Brassicas as well as the petioles of grapevines were modelled by cylinder shapes and the grapevines' leaves were modelled by cuboids. The CC results for different categories, i.e. easy, moderate and difficult, are detailed in Table 2. Table 2 also reports the performance of different techniques under zero-mean white random Gaussian noise with standard deviation value of 0.05. The CCs of the baseline averaging and the SVD technique for the angle estimation task are low. Table 2 shows that these techniques failed to properly model the organs. Since they model the point clouds indirectly via planes, they cannot be used for estimating the diameters. Compared to the above-mentioned methods, bounding-box yields better results, especially for the easy samples. However, the bounding box method still suffers from outliers or highly complicated samples in the moderate and the difficult samples while our technique successfully works under all tested conditions. The proposed method gives the best results in all the tasks over both datasets. The CC results of PC-RANSAC are above 0.90 across all sample types, indicating the robustness of the method to the imaging noise and outliers.

The CC and RRMSE results over all three variants of samples are shown in Figs. 5, 6 and 7. Bounding-box performs well for the diameter and angle estimation in the easy scenario but its performance drastically decreases in the moderate and difficult scenarios. As shown in Fig. 6, in the moderate and difficult settings, the deviation of bounding-box results from the ideal values (dotted diagonal lines) is high, specifically for

Table 2: Correlation coefficient between the estimated parameters and the manual measurements using different methods over both the noise-free and the noisy data. The results over the noisy data are reported in parenthesis.

Method	Leaf angle (Grapevine)	Branch angle (Brassica)	Stem diameter (Brassica)	Branch diameter (Brassica)
Easy				
Averaging	0.453 (0.442)	0.462 (0.451)	-	-
SVD	0.745 (0.723)	0.757 (0.740)	-	-
Bounding-Box	0.867 (0.851)	0.887 (0.871)	0.914 (0.823)	0.906 (0.812)
Ours	0.948 (0.941)	0.953 (0.947)	0.962 (0.941)	0.951 (0.936)
Moderate				
Averaging	0.312 (0.301)	0.322 (0.314)	-	-
SVD	0.483 (0.470)	0.493 (0.488)	-	-
Bounding-Box	0.582 (0.571)	0.596 (0.578)	0.622 (0.548)	0.606 (0.519)
Ours	0.935 (0.929)	0.942 (0.937)	0.945 (0.926)	0.931 (0.914)
Difficult				
Averaging	0.112 (0.107)	0.128 (0.119)	-	-
SVD	0.280 (0.277)	0.289 (0.281)	-	-
Bounding-Box	0.311 (0.298)	0.327 (0.302)	0.337 (0.291)	0.325 (0.280)
Ours	0.912 (0.906)	0.924 (0.917)	0.927 (0.911)	0.916 (0.905)

angles above 60 degrees. The similar behaviour can be seen in the diameter estimation in Fig. 7, where the bounding-box method could not successfully handle the moderate and difficult samples. The overall CCs of the PC-RANSAC results are the highest among the techniques. The distance (RRMSE results) between the PC-RANSAC results and the dotted diagonal lines in the given figures shows a compact even distribution across all angles and diameters, indicating its high accuracy in modelling the organs regardless of their angle and diameter values. We also observe that our technique is less affected by noise (Figs. 6 and 7(b)).

Some results obtained by our proposed and bounding-box methods are illustrated in Figs. 8 and 9. We did not show the results of the averaging and the SVD methods due to their poor performance. Figs. 8 and 9 illustrate that the bounding-box method is highly sensitive to the outliers and its results are unpredictable under partial external disturbance. This aspect of the bounding-box technique is not favourable since the segmentation and clustering results in the point cloud are always accompanied with irrelevant points and measurement techniques must be resistant to such nuisance. The visual results of our method are seen to be consistent with the quantitative results reported in Table 2 and its performance remains almost unchanged under imaging noise, outliers and any other external disturbances, making it reliable for practical phenotyping tasks.
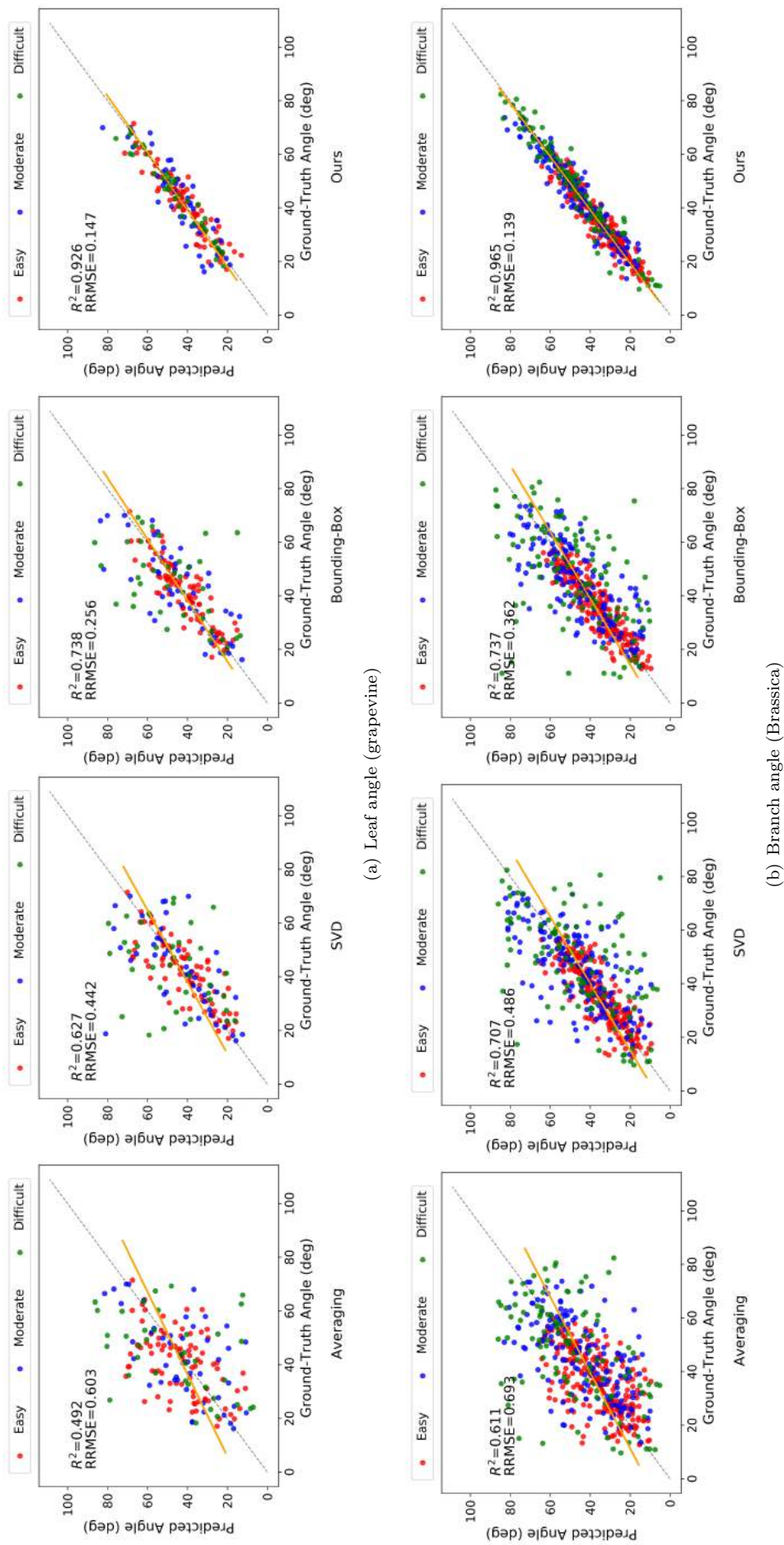
Figure 5: CC and RRMSE between the manual measurements and the estimated angles using different methods in the absence of noise.
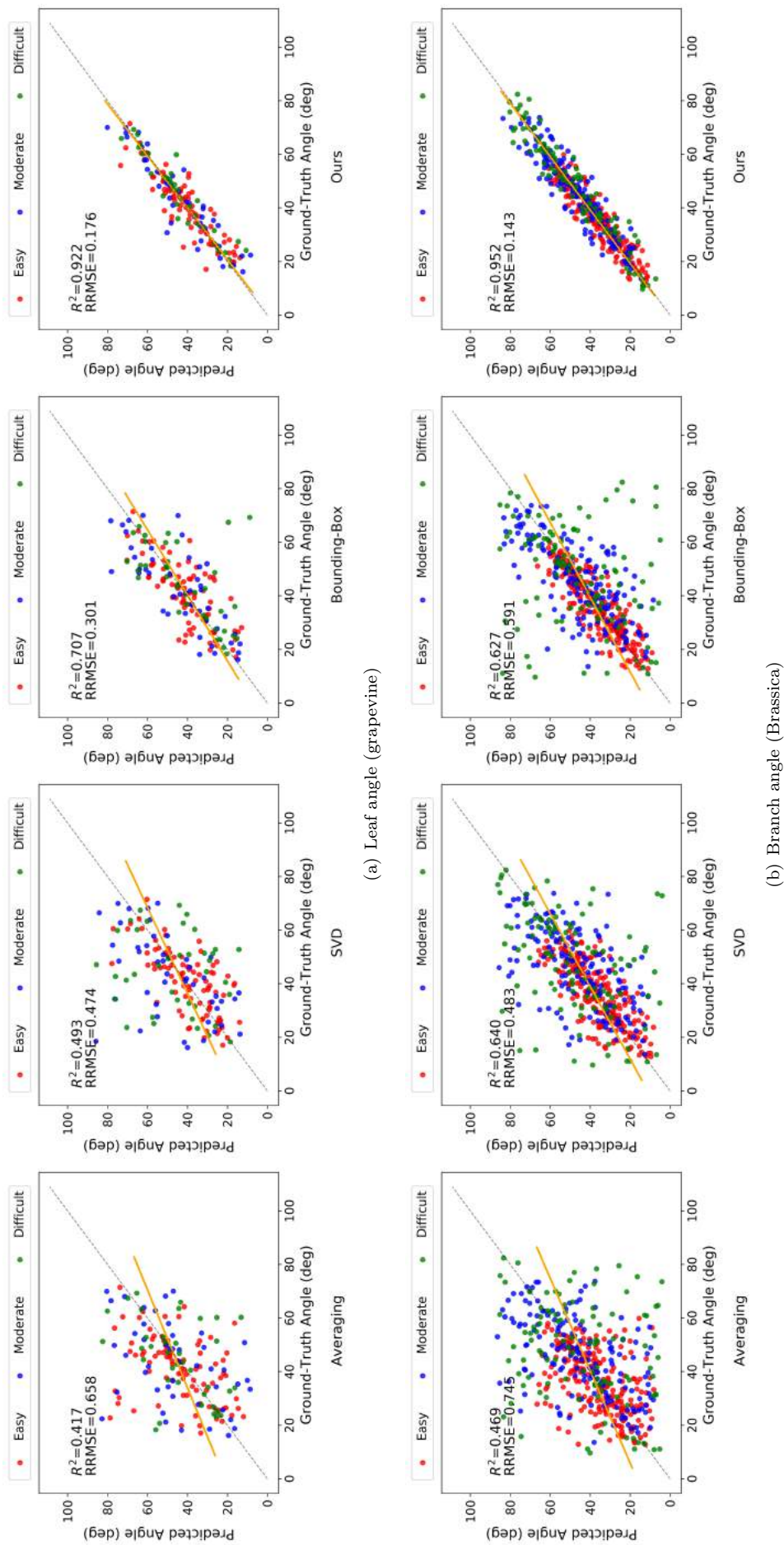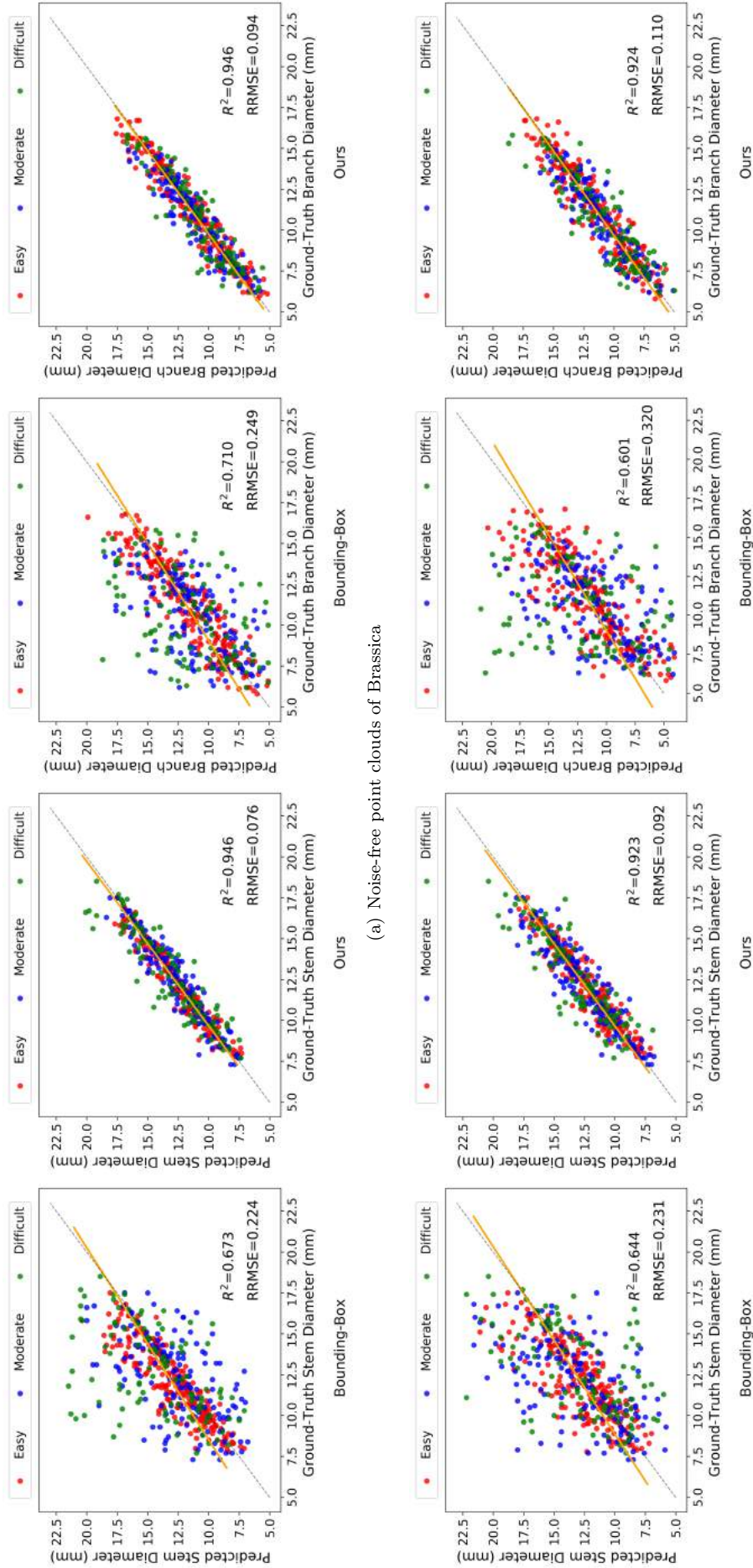
(a) Leaf angle (grapevine)

(b) Branch angle (Brassica)

(a) Leaf angle (grapevine)

(b) Branch angle (Brassica)

Figure 6: CC and RRMSE between the manual measurements and the estimated angles using different methods in the presence of noise.

(a) Noise-free point clouds of Brassica

(b) Noisy point clouds of Brassica

Figure 7: CC and RRMSE between the estimated stem & branch diameters and the manual measurements of the Brassica using different methods.
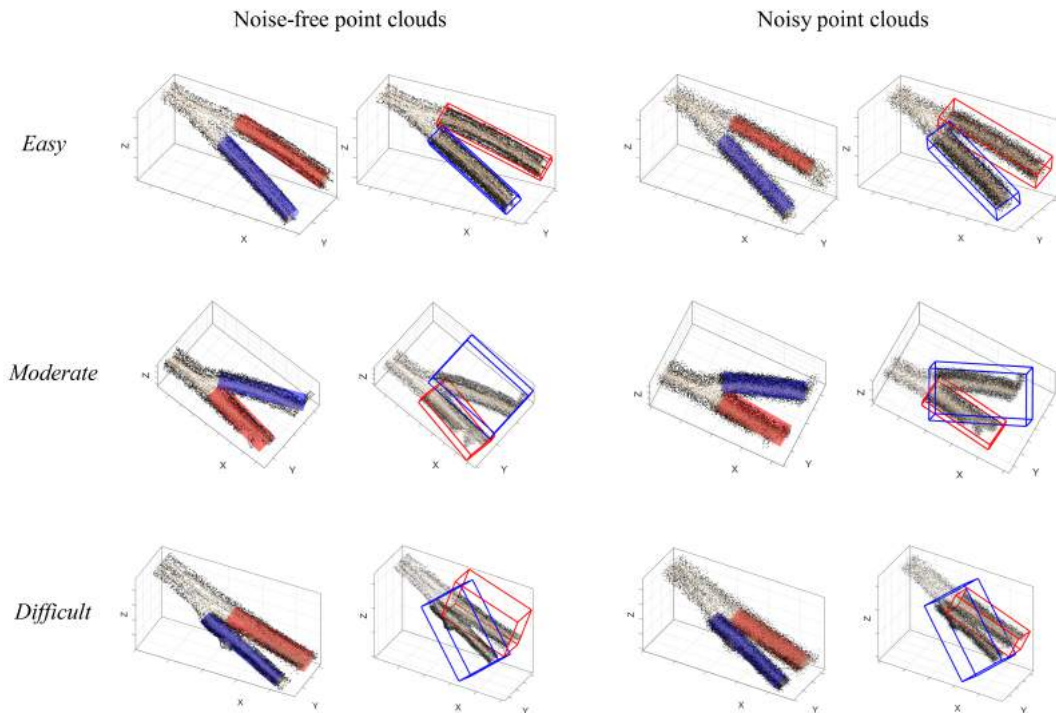
Figure 8: Phenotyping results of the Brassica dataset using our proposed technique (left-hand side) and the bounding-box technique (right-hand side).

4.3 Ablation study and running time

Here we investigate the influence of the predetermined parameters on the performance of our PC-RANSAC algorithm and report its running time. All the following experiments were conducted on 300 samples from all three easy, moderate and difficult categories of both the Brassica and the grapevine datasets.

The experiments were carried out on a 64-bits computer with Core-i7 Intel(R) 6130 CPU @ 2.10GHz processors and the code was implemented in MATLAB (R2018b, version 9.5)[††] without using any boosting libraries.

The accuracy of the results was computed by the relative error metric. If t_{pred} and t_{gt} denote the predicted parameter and the ground-truth measurement respectively, the relative error for parameter t is defined as:

$$e_t = \frac{|t_{pred} - t_{gt}|}{t_{gt}} \times 100\%. \tag{13}$$

We reported the average of relative errors over the 300 samples.

In Eq. 6, it is mentioned that the objective probability $P(n_i, k)$ must be equal or greater than the predetermined probability threshold P_t. We ran the experiment for various values of P_t ranging from 0.7 to 0.99 with intervals of 0.01 and depict the relative errors of the estimated angles as well as their corresponding running time in Fig. 10. The relative errors oscillate when P_t is less than 0.8, and $P_t \geq 0.95$ is the best possible values for the probability threshold, due to the random sampling nature. The running time, on the other hand, is increased gradually for larger thresholds, rendering more iterations (or equivalently, larger k_{min}), as expected.

To increase the confidence of the results, the PC-RANSAC algorithm is repeated R times. Fig. 11 shows the influence of this parameter. When the number of repetitions is less than 30, the results fluctuate considerably. However, the error margin is less than 3% in some cases, highlighting the randomness of the PC-RANSAC algorithm. The figure states that the error margin is less than 3% for $R \geq 30$ and for this reason, this parameter was fixed as 31 throughout this study. Finally, the impact of the number of input points on the accuracy of the estimated angle is reported in Fig. 12. This parameter heavily relies on the complexity of given point clouds: more than 4k points provide an error margin of less than 2%. Contrary to the previous results, the running time is almost unchanged and independent of the number n_s of input points, since the repetition k of the steps in the proposed PC-RANSAC algorithm was determined by the probability of inliers, but not by the actual number n_s of the points in the given point cloud in Eq. 7. This confirms
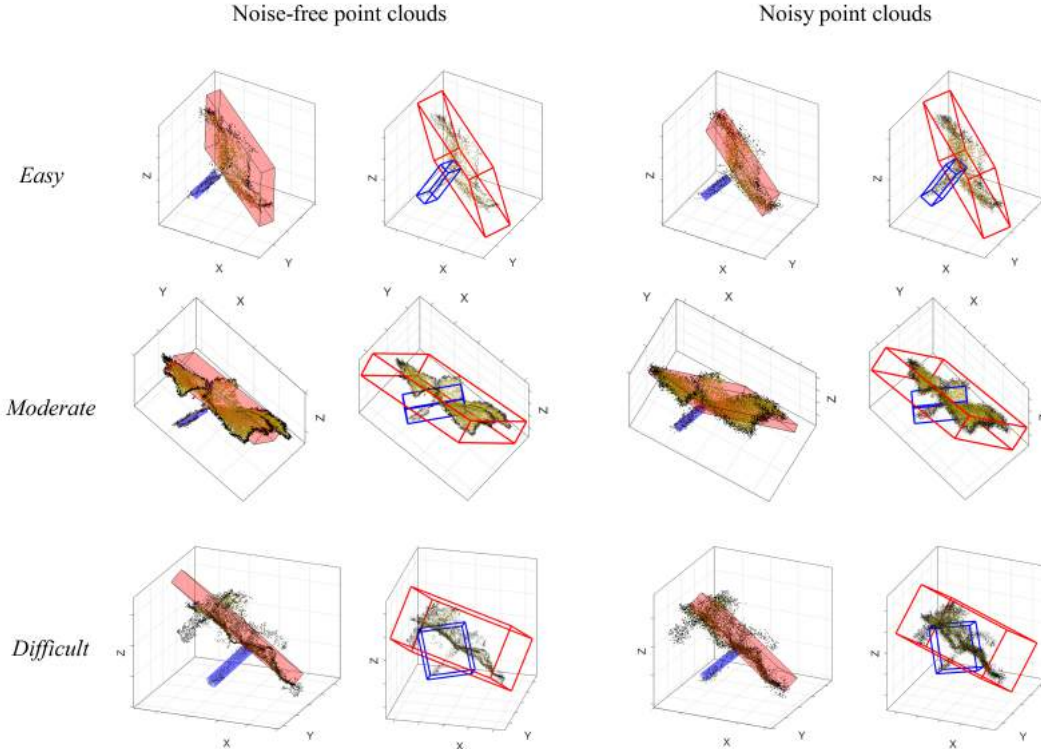

[††]`https://www.mathworks.com`

Figure 9: Phenotyping results of the grapevine dataset using our proposed technique (left-hand side) and the bounding-box technique (right-hand side).

that high-resolution point clouds could result in better results. In short, the ablation study suggests that the best values for P_t, R and the number of points are 0.99, 31 and 16K respectively, as done for the Brassica and grapevine experiments in the preceding section. This setting requires 43.2 seconds for processing each point cloud sample on a 64-bits computer with Core-i7 Intel(R) 6130 CPU @ 2.10GHz processor.

5   Conclusion and Future Work

The goal of this work was to utilise irregular point clouds directly for measuring attributes of organs for plant phenotyping, handling noise, distortions and any irrelevant data. We have extracted diameter and angle measurements using the point cloud random sample consensus (PC-RANSAC) algorithm. The tissues were modelled using cylinder and cuboid shapes and the shapes were then fitted onto the organs by the PC-RANSAC algorithm. The estimated shapes must contain the majority of inlier points and discard the outliers. The presence of outliers in the point cloud is almost inevitable and this should be taken into account. The proposed technique is specifically designed for the analysis of point clouds of plants and avoids the need to transfer information to other domains. This reduces the processing time as well as the uncertainty of transferred data, resulting in reliable measurements. Experimental results and a comparative study with the existing techniques over two datasets showed that the proposed method can successfully measure parameters of interest ($R^2 > 0.91$) and is also robust to imaging noise and outliers ($R^2 > 0.90$).

Investigating the effectiveness of the proposed method for shoot and root branch growth angle modeling would be interesting. Defining the complex morphology of plants needs a large number of geometric parameters. In this report, we show that the proposed technique can be applied to such plants. To this end, the organs of interest must be modeled by appropriate geometrical shapes. We believe that there is still room for enhancing the results reported here. For example, in this study, the leaf was modeled as a cuboid as our primary aim was to extract angle. The ability to accurately capture area and shape traits could be improved by replacing the cuboid restriction with a more realistic and flexible shape like [52]. Complex organs need higher degrees-of-freedom and cannot be modeled by a simple cylinder or a cuboid. Our ultimate goal is to produce a highly efficient GPU & multithreaded processors implementation for real-time measurements of the parameters of plants of interest.
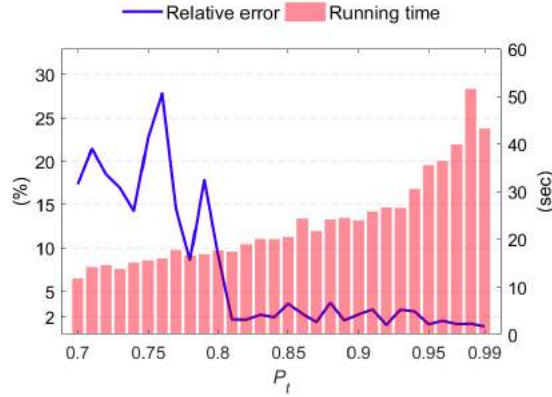
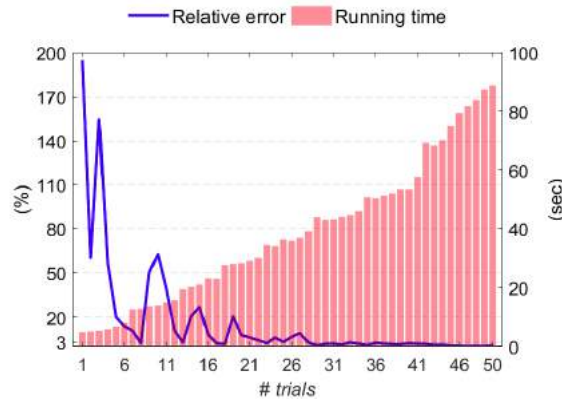Figure 10: Influence of the predetermined probability threshold P_t on the accuracy of the estimated angles.

Figure 11: Influence of the number of trials on the accuracy of the estimated angles.

ACKNOWLEDGMENTS

References

[1] L. Cooper, A. Meier, M.-A. Laporte, J. L. Elser, C. Mungall, B. T. Sinn, D. Cavaliere, S. Carbon, N. A. Dunn, B. Smith, et al., The planteome database: an integrated resource for reference ontologies, plant genomics and phenomics, Nucleic acids research 46 (D1) (2018) D1168–D1180.

[2] A. Hamidinekoo, G. A. Garzón-Martínez, M. Ghahremani, F. M. Corke, R. Zwiggelaar, J. H. Doonan, C. Lu, Deeppod: a convolutional neural network based quantification of fruit number in arabidopsis, GigaScience 9 (3) (2020) giaa012.

[3] G. Bernotas, L. C. Scorza, M. F. Hansen, I. J. Hales, K. J. Halliday, L. N. Smith, M. L. Smith, A. J. McCormick, A photometric stereo-based 3d imaging system using computer vision and deep learning for tracking plant growth, GigaScience 8 (5) (2019) giz056.

[4] J. Gené-Mola, R. Sanz-Cortiella, J. R. Rosell-Polo, J.-R. Morros, J. Ruiz-Hidalgo, V. Vilaplana, E. Gregorio, Fruit detection and 3d location using instance segmentation neural networks and structure-from-motion photogrammetry, Computers and Electronics in Agriculture 169 (2020) 105165.

[5] Y. Le Cozler, C. Allain, C. Xavier, L. Depuille, A. Caillot, J. Delouard, L. Delattre, T. Luginbuhl, P. Faverdin, Volume and surface area of holstein dairy cows calculated from complete 3d shapes acquired
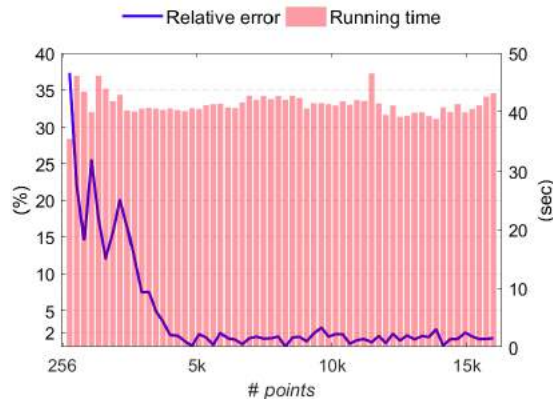
Figure 12: Influence of the number of input 3D points on the accuracy of the estimated angles.

using a high-precision scanning system: Interest for body weight estimation, Computers and Electronics in Agriculture 165 (2019) 104977.

[6] L. E. Gangsei, J. Kongsro, Automatic segmentation of computed tomography (ct) images of domestic pig skeleton using a 3d expansion of dijkstra's algorithm, Computers and Electronics in Agriculture 121 (2016) 191–194.

[7] T. Dong, X. Zhang, Z. Ding, J. Fan, Multi-layered tree crown extraction from lidar data using graph-based segmentation, Computers and Electronics in Agriculture 170 (2020) 105213.

[8] W. Fang, H. Feng, W. Yang, L. Duan, G. Chen, L. Xiong, Q. Liu, High-throughput volumetric reconstruction for 3d wheat plant architecture studies, Journal of Innovative Optical Health Sciences 9 (05) (2016) 1650037.

[9] H. Cuevas-Velasquez, A.-J. Gallego, R. B. Fisher, Segmentation and 3d reconstruction of rose plants from stereoscopic images, Computers and electronics in agriculture 171 (2020) 105296.

[10] W. Gélard, M. Devy, A. Herbulot, P. Burger, Model-based segmentation of 3d point clouds for phenotyping sunflower plants, in: 12. International Joint Conference on Computer Vision, Imaging and Computer Graphics Theory and Applications, 2017.

[11] S. Paulus, J. Dupuis, A.-K. Mahlein, H. Kuhlmann, Surface feature based classification of plant organs from 3d laserscanned point clouds for plant phenotyping, BMC bioinformatics 14 (1) (2013) 238.

[12] F. Hétroy-Wheeler, E. Casella, D. Boltcheva, Segmentation of tree seedling point clouds into elementary units, International Journal of Remote Sensing 37 (13) (2016) 2881–2907.

[13] D. Zermas, V. Morellas, D. Mulla, N. Papanikolopoulos, 3d model processing for high throughput phenotype extraction–the case of corn, Computers and Electronics in Agriculture 172 (2020) 105047.

[14] S. Vijayarangan, P. Sodhi, P. Kini, J. Bourne, S. Du, H. Sun, B. Poczos, D. Apostolopoulos, D. Wettergreen, High-throughput robotic phenotyping of energy sorghum crops, in: Field and Service Robotics, Springer, 2018, pp. 99–113.

[15] M. Ghahremani, K. Williams, F. M. K. Corke, B. Tiddeman, Y. Liu, J. H. Doonan, Deep segmentation of point clouds of wheat, Frontiers in Plant Science 12 (2021) 429.

[16] A. Chaudhury, C. Godin, Skeletonization of plant point cloud data using stochastic optimization framework, Frontiers in Plant Science 11 (2020).

[17] N. Briglia, K. Williams, D. Wu, Y. Li, S. Tao, F. Corke, G. Montanaro, A. Petrozza, D. Amato, F. Cellini, et al., Image-based assessment of drought response in grapevines, Frontiers in Plant Science 11 (2020) 595.

[18] J. Qi, D. Xie, L. Li, W. Zhang, X. Mu, G. Yan, Estimating leaf angle distribution from smartphone photographs, IEEE Geoscience and Remote Sensing Letters 16 (8) (2019) 1190–1194.

[19] A. A. Chaugule, S. N. Mali, Identification of paddy varieties based on novel seed angle features, Computers and Electronics in Agriculture 123 (2016) 415–422.

[20] J. L. Schönberger, J.-M. Frahm, Structure-from-motion revisited, in: IEEE/CVF Conference on Computer Vision and Pattern Recognition (CVPR), 2016.

[21] M. Ghahremani, Y. Liu, B. Tiddeman, Ffd: Fast feature detector, IEEE Transactions on Image Processing 30 (2020) 1153–1168.

[22] C. Wu, Visualsfm: A visual structure from motion system, Mechanism and Machine Theory 92 (2011) 144–152.

[23] S. Paulus, Measuring crops in 3d: using geometry for plant phenotyping, Plant Methods 15 (1) (2019) 1–13.

[24] K. Panjvani, A. V. Dinh, K. A. Wahid, Lidarpheno–a low-cost lidar-based 3d scanning system for leaf morphological trait extraction, Frontiers in plant science 10 (2019) 147.

[25] M. Shindo, S. Yamamoto, K. Shimomura, M. Umehara, Strigolactones decrease leaf angle in response to nutrient deficiencies in rice, Frontiers in plant science 11 (2020) 135.

[26] D. Wu, D. Wu, H. Feng, L. Duan, G. Dai, X. Liu, K. Wang, P. Yang, G. Chen, A. P. Gay, et al., A deep learning-integrated micro-ct image analysis pipeline for quantifying rice lodging resistance-related traits, Plant Communications (2021) 100165.

[27] Y. Xu, R. Zhang, Z. Hou, C. Yan, X. Xia, C. Ma, S. Dong, Z. Gong, Mechanical properties of soybean plants under various plant densities, Crop and Pasture Science 71 (3) (2020) 249–259.

[28] J. Kirchner, A. Robaina, M. Peiter, R. Torres, W. Mezzomo, R. Rosso, et al., Height of plants and diameter of stems of sorghum forage irrigated by cuts., IRRIGA 25 (2) (2020) 223–233.

[29] D. T. Melese, Effect of diameter, root moisture content, gauge length and loading rate on tensile strength of plant roots and their contribution to slope stability, Lowland Technology International 22 (4) (2021).

[30] M. Furutani, Y. Hirano, T. Nishimura, M. Nakamura, M. Taniguchi, K. Suzuki, R. Oshida, C. Kondo, S. Sun, K. Kato, et al., Polar recruitment of rld by lazy1-like protein during gravity signaling in root branch angle control, Nature communications 11 (1) (2020) 1–13.

[31] H. Li, L. Zhang, J. Hu, F. Zhang, B. Chen, K. Xu, G. Gao, H. Li, T. Zhang, Z. Li, et al., Genome-wide association mapping reveals the genetic control underlying branch angle in rapeseed (brassica napus l.), Frontiers in plant science 8 (2017) 1054.

[32] M. Bemer, H. van Mourik, J. M. Muiño, C. Ferrándiz, K. Kaufmann, G. C. Angenent, Fruitfull controls saur10 expression and regulates arabidopsis growth and architecture, Journal of experimental botany 68 (13) (2017) 3391–3403.

[33] S. Liu, F. Baret, B. Andrieu, P. Burger, M. Hemmerle, Estimation of wheat plant density at early stages using high resolution imagery, Frontiers in Plant Science 8 (2017) 739.

[34] B. Wang, S. M. Smith, J. Li, Genetic regulation of shoot architecture, Annual review of plant biology 69 (2018) 437–468.

[35] K. A. Levin, S. A. Boden, A new branch of understanding for barley inflorescence development, Journal of Experimental Botany 71 (22) (2020) 6869–6871.

[36] A. Trewavas, The foundations of plant intelligence, Interface focus 7 (3) (2017) 20160098.

[37] J. Pisek, Y. Ryu, K. Alikas, Estimating leaf inclination and g-function from leveled digital camera photography in broadleaf canopies, Trees 25 (5) (2011) 919–924.

[38] L. Lou, Y. Liu, M. Shen, J. Han, F. Corke, J. H. Doonan, Estimation of branch angle from 3d point cloud of plants, in: 2015 International Conference on 3D Vision, IEEE, 2015, pp. 554–561.

[39] J. Li, L. Tang, Developing a low-cost 3d plant morphological traits characterization system, Computers and Electronics in Agriculture 143 (2017) 1–13.

[40] M. Li, L. L. Klein, K. E. Duncan, N. Jiang, D. H. Chitwood, J. P. Londo, A. J. Miller, C. N. Topp, Characterizing 3d inflorescence architecture in grapevine using x-ray imaging and advanced morphometrics: implications for understanding cluster density, Journal of experimental botany 70 (21) (2019) 6261–6276.

[41] M. Li, M.-R. Shao, D. Zeng, T. Ju, E. A. Kellogg, C. N. Topp, Comprehensive 3d phenotyping reveals continuous morphological variation across genetically diverse sorghum inflorescences, New Phytologist 226 (6) (2020) 1873–1885.

[42] H. Wang, D. Mirota, G. D. Hager, A generalized kernel consensus-based robust estimator, IEEE transactions on pattern analysis and machine intelligence 32 (1) (2009) 178–184.

[43] M. A. Fischler, R. C. Bolles, Random sample consensus: a paradigm for model fitting with applications to image analysis and automated cartography, Communications of the ACM 24 (6) (1981) 381–395.

[44] R. Schnabel, R. Wahl, R. Klein, Efficient ransac for point-cloud shape detection, in: Computer graphics forum, Vol. 26, Wiley Online Library, 2007, pp. 214–226.

[45] L. Li, F. Yang, H. Zhu, D. Li, Y. Li, L. Tang, An improved ransac for 3d point cloud plane segmentation based on normal distribution transformation cells, Remote Sensing 9 (5) (2017) 433.

[46] M. Ghahremani, Y. Liu, Y. Zhao, L. Ai, R. Song, R. Martin, L. Chen, X. Ren, L. Li, Rigid Registration, Springer International Publishing, Cham, 2020, pp. 1–13.

[47] Y.-H. Jin, W.-H. Lee, Fast cylinder shape matching using random sample consensus in large scale point cloud, Applied Sciences 9 (5) (2019) 974.

[48] M. Mishima, H. Uchiyama, D. Thomas, R.-i. Taniguchi, R. Roberto, J. P. Lima, V. Teichrieb, Incremental 3d cuboid modeling with drift compensation, Sensors 19 (1) (2019) 178.

[49] P. H. Torr, A. Zisserman, Mlesac: A new robust estimator with application to estimating image geometry, Computer vision and image understanding 78 (1) (2000) 138–156.

[50] J. S. Dai, Euler–rodrigues formula variations, quaternion conjugation and intrinsic connections, Mechanism and Machine Theory 92 (2015) 144–152.

[51] J. L. Schönberger, E. Zheng, M. Pollefeys, J.-M. Frahm, Pixelwise view selection for unstructured multi-view stereo, in: European Conference on Computer Vision (ECCV), 2016.

[52] W. Wen, B. Li, B.-j. Li, X. Guo, A leaf modeling and multi-scale remeshing method for visual computation via hierarchical parametric vein and margin representation, Frontiers in plant science 9 (2018) 783.